remote sensing

MDPI

Article

Four Dimensional Mapping of Vegetation Moisture Content Using Dual-Wavelength Terrestrial Laser Scanning

Ahmed Elsherif [1,2,*], Rachel Gaulton [3] and Jon Mills [1]

1 School of Engineering, Newcastle University, Newcastle Upon Tyne NE1 7RU, UK; jon.mills@newcastle.ac.uk
2 Faculty of Engineering, Tanta University, Tanta 31733, Egypt
3 School of Natural and Environmental Sciences, Newcastle University, Newcastle Upon Tyne NE1 7RU, UK; rachel.gaulton@newcastle.ac.uk
* Correspondence: a.m.a.elsherif2@newcastle.ac.uk

Received: 30 August 2019; Accepted: 1 October 2019; Published: 4 October 2019

Abstract: Recently, terrestrial laser scanning (TLS) has shown potential in measuring vegetation biochemical traits in three dimensions (3D) by using reflectance derived from backscattered intensity data. The 3D estimates can provide information about the vertical heterogeneity of canopy biochemical traits which affects canopy reflectance but cannot be measured from spaceborne and airborne optical remote sensing data. Leaf equivalent water thickness (EWT), a metric widely used in vegetation health monitoring, has been successfully linked to the normalized difference index (NDI) of near and shortwave infrared wavelengths at the leaf level. However, only two previous studies have linked EWT to NDI at the canopy level in field campaigns. In this study, an NDI consisting of 808 and 1550 nm wavelengths was used to generate 3D EWT estimates at the canopy level in a broadleaf mixed-species tree plot during and after a heatwave. The relative error in EWT estimates was 6% across four different species. Temporal changes in EWT were measured, and the accuracy varied between trees, a factor of the errors in EWT estimates on both dates. Vertical profiles of EWT were generated for six trees and showed vertical heterogeneity and variation between species. The change in EWT vertical profiles during and after the heatwave differed between trees, demonstrating that trees reacted in different ways to the drought condition.

Keywords: Lidar; water stress; leaf water content; drought; vegetation

1. Introduction

Global warming has been linked to the recent increase in the frequency and intensity of heatwaves, with climate models predicting more heatwaves to occur in the future [1]. Heatwaves, when accompanied by lack of rainfall, can trigger severe drought conditions with catastrophic effects on the agricultural and forestry sectors, reducing crop yields and increasing the rates of forest fires and tree mortality [2]. For instance, the record-breaking 2003 European heatwave caused a fall in arable crop production by more than 10% (23 million tons, the highest recorded drop in a century) in comparison to the previous year [3]. In addition, more than twenty-five thousand forest fires were reported across Europe, destroying approximately 730 thousand hectares of forests [3]. A total estimated loss of approximately 13 billion Euros was reported, resulting from the loss in agricultural and livestock sectors, in addition to the impact of forest fires [3]. Stott, et al. [4] estimated that the risk of occurrence of the 2003 European heatwave was doubled because of the increase in greenhouse gases concentrations in the atmosphere caused by human activities. Similarly, Vogel, et al. [5] identified human-caused climate change as a factor that increased the magnitude of the 2018 European heatwave. Recently, the heatwave that hit Europe in June and July 2019 broke the highest temperature records set by the 2003 heatwave [6].

During drought, plants use different survival mechanisms, one of which is closing leaf stomata (pores on the underside of leaves) to minimize water loss, which reduces the plant transpiration rate [7]. Transpiration refers to water movement through a plant from roots to leaves to distribute water and nutrients needed for photosynthesis before water gets evaporated through leaf stomata [8]. Stomatal closure further affects the plant photosynthetic rate by limiting carbon dioxide intake [9]. The drop in the rates of transpiration, photosynthesis, and carbon gain cause a decline in plant growth rate and productivity, and the plant also becomes more prone to burning [10]. If drought conditions are prolonged, the plant may eventually suffer from carbon starvation or hydraulic failure, leading to its death [11]. The continuous monitoring of vegetation water status can lead to the early detection of vegetation stress, which can help in improving decision making related to crop irrigation and harvesting during droughts [12] and in preventing and fighting forest fires [13].

Vegetation water status metrics can be retrieved at the landscape level using data from multispectral and hyperspectral optical remote sensing (RS) spaceborne sensors, and times series of data can be produced to monitor changes in vegetation moisture content [14]. Leaf equivalent water thickness (EWT), the amount of water in leaf per unit leaf surface area, is a widely-used metric in the RS of vegetation health because it can be estimated directly from reflectance in the optical domain [15]. Estimating EWT from optical RS data is based on the interaction of radiation with foliage in the short wave infrared (SWIR) wavelengths being dominated by absorption by water, where reflected energy is negatively related to leaf water content [16,17]. However, SWIR reflectance alone is insufficient to accurately retrieve EWT, as leaf internal structure also affects SWIR reflectance [7]. Combining near infrared (NIR) and SWIR reflectance in vegetation indices can minimize leaf internal structure effects and thus lead to a more accurate estimation of EWT [7,15,18]. Numerous vegetation indices have been developed and successfully linked to EWT, e.g., the normalized difference infrared index (NDII) [19], the normalized difference water index (NDWI) [20], the water index (WI) [21], and the moisture stress index (MSI) [18] (Table 1). Variations of the aforementioned indices have also been developed using different wavelength combinations, and these have been successfully linked to EWT [15,22–24].

Table 1. Vegetation water status indices.

Index	Formula
NDII	$(P_{820} - P_{1650})/(P_{820} + P_{1650})$
NDWI	$(P_{860} - P_{1240})/(P_{860} + P_{1240})$
WI	$(P_{900})/(P_{970})$
MSI	$(P_{1600})/(P_{820})$

Vegetation indices are sensor specific and dependent on site and sampling conditions [13,16,25]. At the landscape level, the performance of vegetation indices is also influenced by canopy structure, understory vegetation, soil moisture content, non-photosynthetic components, atmospheric conditions, solar illumination and sensor viewing angles [17,26–29]. Radiative transfer models (RTMs) can overcome these limitations, as they are not site-dependent and can take the characteristics of leaf biophysical and biochemical traits, canopy structure, and background soil into consideration. By inverting these models, EWT and other canopy characteristics can be estimated [15,17,30–32].

Estimating EWT from spaceborne and airborne optical RS data, despite its advantages over in situ approaches, has some limitations. The temporal resolution of optical RS spaceborne sensors may not be suitable for monitoring rapid changes in vegetation water status, while cloud coverage can further reduce temporal resolution [33]. The spatial resolution of open access spaceborne sensors, such as Landsat and MODIS (Moderate-Resolution Imaging Spectroradiometer), can also be a limiting factor in heterogeneous canopy areas where a single pixel may combine the spectral responses of different species or land covers [34]. Optical RS sensors also cannot measure EWT predawn, which is a more reliable indicator of water stress than midday EWT because there is no transpiration occurring [35]. Furthermore, the vertical heterogeneity of EWT within canopies, as well as other biochemical and biophysical traits, cannot be studied using optical RS data, although such heterogeneity plays an important role in canopy reflectance [36]. For instance, Kuusk [37] and Wang, et al. [36] reported that ignoring such heterogeneity while using radiative transfer modelling to retrieve vegetation traits from optical RS data can cause significant errors in sites with large vertical and/or horizontal canopy heterogeneity.

Recently, terrestrial laser scanning (TLS) has emerged as a promising tool to estimate vegetation biochemical traits in three dimensions, using the recorded backscattered intensity data, after decades of being solely used to measure vegetation structural parameters. TLS intensity data can be linked to leaf reflectance via radiometric correction and then used to retrieve leaf biochemical traits, a factor of utilizing a suitable wavelength, such as SWIR if estimating EWT (for more about TLS intensity data calibration, see the work of Elsherif, et al. [38]). Zhu, et al. [39] showed that a single-wavelength TLS instrument equipped with a 1550 nm SWIR wavelength could accurately estimate EWT at the canopy level in a controlled indoors environment. However, transferring the method to a real forest environment is complicated by the incidence angle effects and the angle between the incident laser beam and object surface normal, both of which alter the intensity value [40]. The accuracy of EWT estimates depends mainly on how accurately the incidence angle for each point in the point-cloud is calculated, a challenging process in a complex vegetation canopy [40]. In a mixed-species tree plot, the variation in leaf structure, mainly leaf thickness and leaf mass per area (LMA, leaf dry weight per unit leaf surface area), can further complicate the retrieval of EWT using a single wavelength, because these parameters affect the SWIR reflectance [41].

To overcome the limitations of single-wavelength TLS, multispectral and hyperspectral TLS systems have been developed (typically non-commercial systems built for scientific research) which allow for the calculation of spectral indices that can be linked to leaf biochemical traits [42]. Hancock, et al. [40] showed that using the normalized difference index (NDI) of NIR and SWIR can minimize incidence angle effects, and Gaulton, et al. [43] reported a high correlation between NDI and EWT at the leaf level. However, no successful attempts to utilize such systems to estimate EWT at the canopy level in field campaigns have been reported in the literature, as these systems are still considered proof-of-concept. Junttila, et al. [44] and Elsherif, et al. [38] showed that intensity data from commercially-available NIR and SWIR TLS systems can be combined to calculate the NDI, reporting a high correlation between the NDI and EWT at the leaf level for coniferous and broadleaf species, respectively. At the canopy level, Junttila, et al. [45] used an NDI of 905 and 1550 nm wavelengths with the FARO S120 and FARO X330 TLS instruments, respectively, to detect European spruce bark beetle infestation symptoms in 29 mature Norway spruce trees. The trees were successfully classified into three classes (no, low, and moderate infestation levels) with an overall accuracy of 66%. Elsherif, et al. [46] used an NDI of 808 and 1550 nm wavelengths with the Leica P20 and Leica P40 TLS instruments, respectively, to generate 3D EWT estimates at the canopy level in a mixed-species broadleaf forest plot; they reported EWT vertical heterogeneity in all sampled 13 trees. To our knowledge, no other studies have successfully estimated EWT at the canopy level in field campaigns using TLS, and no previous studies have used TLS to monitor changes in EWT.

This study used the same scanning methodology described by Elsherif, et al. [46] to investigate the potential of using dual-wavelength TLS to monitor temporal changes in EWT at the canopy level in 3D. A mixed-species tree plot was scanned twice, during and after the 2018 European heatwave. An NDI of 808 and 1550 nm wavelengths with the Leica P20 and P50 commercial TLS instruments, respectively, was used to generate 3D EWT point-clouds on both dates. The aims of the study were to: (i) Investigate how accurately the temporal changes in EWT can be measured using TLS, (ii) study how EWT vertical profiles varied between species, and (iii) examine the temporal changes in EWT vertical profiles during and after the heatwave.

2. Materials and Methods

2.1. TLS Instruments

The Leica P20 and P50 instruments (Figure 1) are commercial, time-of-flight, pulsed TLS systems. Their technical specifications are given in Table 2. The Leica P20 utilizes the 808 nm near infrared wavelength, while the Leica P50 operates at the 1550 nm shortwave infrared wavelength. The NDI of the two wavelengths can minimize incidence angle effects [38] and leaf internal structure effects [46] with no need for additional radiometric corrections. Furthermore, point-clouds from the two instruments can be aligned with a high accuracy, allowing for the calculation of the NDI on a point-by-point basis as a result of the similarities between the instruments' laser beam exit locations, chassis, and scanning mechanisms [47]. Methods to calibrate the intensity data to apparent reflectance using external reference targets with a known reflectance have been successfully developed for the Leica P20 [38,46] and the Leica P50 [47]. The intensity correction models described in the aforementioned studies were used to calibrate the intensity to apparent reflectance in all experiments described in this study.


(**a**) (**b**)

Figure 1. The TLS instruments used in this study: (**a**) The Leica P20 and (**b**) the Leica P50. The similarities in chassis, laser beam exit locations, and scanning mechanisms allow for the high registration accuracy of the point-clouds from the two instruments.

Table 2. Technical specifications of the Leica P20 and P50 terrestrial laser scanning (TLS) instruments.

	Leica P20	**Leica P50**
Measurement type	time-of-flight	time-of-flight
Wavelength	808 nm	1550 nm
Maximum range	120 m at 18% reflectivity	1 km at 80% reflectivity
Beam diameter at exit	2.8 mm	3.5 mm
Beam diameter at 10 m	4.8 mm	5.8 mm
Beam diameter at 20 m	6.8 mm	8.1 mm
Beam divergence	0.20 mrad	0.23 mrad

2.2. Study Area

The study area was a mixed-species tree plot (35 m × 35 m) in Exhibition Park, Newcastle upon Tyne, UK (54.98° N, 1.62° W). The tree species included: *Ilex aquifolium* (holly), *Acer pseudoplatanus* (sycamore), *Sorbus intermedia* (Swedish whitebeam), *Fraxinus excelsior* (ash), *Aesculus hippocastanum* (horse chestnut), *Fagus sylvatica* (beech), and *Tilia x europaea* (lime). A single scanning position was set in the center of the plot corresponding to a wide gap in canopy cover and aimed at obtaining as many laser beam returns as possible from the canopy top. The scanning position covered nine trees: Two holly trees, two ash trees, two Swedish whitebeam tress, one beech tree, one sycamore tree, and one horse chestnut tree. The horse chestnut tree was suffering from horse-chestnut leaf miner (*Cameraria ohridella*) and thus was excluded from any further processing.

The plot was scanned on 7th of August 2018 in the end of the 2018 heatwave that hit the British Isles between 23rd of June and 7th of August as part of the 2018 European heatwave, making summer 2018 the joint-warmest summer in recorded in the UK and the second warmest summer in the North East England region. Temperatures in Newcastle upon Tyne reached 26 °C, significantly higher than the 15 °C recorded average summer temperature. Scans were conducted with the P20 and P50 instruments, which were mounted consecutively on the same tripod on the same surveying point (scanning position). Three Leica black and white registration targets were placed in the plot at different heights for the purpose of aligning the P20 and P50 point-clouds. A full-hemisphere scan (360° × 270°) was conducted with each instrument with a resolution (point spacing) of 3 mm at 10 m. The duration of the scan was approximately fifteen minutes for each instrument, and ambient conditions were constant during the scans. The plot was scanned again on 22nd of October 2018 while leaves were senescing, using the same scanning set-up. The average temperature in October was 13 °C, with periods of rainfall throughout the month. On each date, leaf samples were collected immediately after scanning to link the TLS data to EWT, as described in Section 2.3.

2.3. Leaf Sampling

On each date, two sets of leaf samples were collected, one for the purpose of building the NDI–EWT estimation model and the other for the validation of the EWT estimates. As the study area was in a public park, extensive destructive sampling of the trees was not possible. The total number of leaf samples collected in the August dataset was 50 samples, while the total number of samples collected in the October dataset was 38 samples. Leaf sampling details are given in Table 3. Samples for building the EWT estimation model were randomly collected from the plot. The aim here was not to derive species-specific models but to build a pooled EWT estimation model on each date. The NDI–EWT relationship was previously reported to be species-independent to an extent [38,46], and the leaf sampling aimed at further investigating this observation. On the other hand, leaf samples for validation were collected from a small volume, approximately 0.5 × 0.5 × 0.5 m, with a known crown location in a specific tree from each species.

Sycamore leaf samples were found to be covered with grey powdery material, indicating that the tree suffered from powdery mildew disease. This severely affected the NDI–EWT relationship as discussed in Sections 3.1 and 3.2, and the tree was thus excluded in October data collection. Leaf samples of holly were thicker than the other species; in addition, they had a glossy, waxy surface. The lime tree was on the edge of the plot, fully occluded by two ash trees, so no leaf samples were collected for validation, and samples were only collected to add species variety to the EWT estimation model in August. In October, the tree had already lost its leaves.

Table 3. Number of leaf samples collected in the August and October datasets.

	August		**October**	
	EWT model	Validation	EWT model	Validation
Swedish whitebeam	5	5	5	5
Ash	3	5	5	4
Beech	6	5	5	5
Holly	4	5	4	5
Sycamore	3	4	—	—
Lime	5	—	—	—
Total number of leaf samples	26	24	19	19

2.4. Leaf Samples Processing and Biochemistry Measurements

This section describes processing the leaf samples to measure their EWT and to derive the NDI–EWT estimation model for the August dataset. The same steps were repeated for the October dataset, and differences, where present, are highlighted. The fresh weight (FW) of each leaf sample was measured using an electronic scale (one milligram precision) immediately upon collection. Afterwards, leaf samples for building the EWT estimation model were mounted on a wooden frame and consecutively scanned with the P20 and P50 instruments at range of 6 m (7 m for the October dataset). The laser beam direction was almost normal to the wooden frame to minimize the incidence angle effects. Next, all leaf samples, for building the EWT estimation model and for validating the estimation, were transferred to the laboratory to measure their surface area (SA). They were scanned with a Epson Perfection photo scanner (600 dpi), and the SA of each leaf was determined using Image-J 1.50i software [48]. The Leaf samples were then left to dry naturally over a period of five days (a week for the October dataset), then were further dried in an oven for 72 h at 60 °C. Holly leaf samples were oven-dried for additional six days until no change in their weight was observed, ensuring that they were fully dry. The dry weight (DW) of each leaf sample was measured using the same scale used to measure the FW, and EWT was calculated according to Equation (1) [49].

$$\text{EWT (g cm}^{-2}\text{)} = (\text{FW} - \text{DW})/\text{SA}, \tag{1}$$

The intensity values of the leaf samples collected for the purpose of building the EWT estimation model were calibrated to apparent reflectance. Afterwards, the NDI of each leaf sample was calculated following Equation (2).

$$\text{NDI} = (\text{P20}_\text{R} - \text{P50}_\text{R})/(\text{P20}_\text{R} + \text{P50}_\text{R}), \tag{2}$$

where P20_R is NIR reflectance, obtained from the P20 intensity data, and P50_R is SWIR reflectance, derived from the P50 intensity data.

Reduced major axis regression was used to derive the NDI–EWT relationships. For the August dataset, different NDI–EWT relationships were examined. Firstly, a pooled NDI–EWT model was fitted to all combined species. Next, the diseased sycamore leaf samples were excluded, and a second pooled NDI–EWT model was fitted to the remaining species. The next step was to exclude holly leaf samples from the pooled EWT model and derive a species-specific EWT estimation model for them in order to account for their thickness and surface characteristics that differed from the remaining species. The remaining leaf samples were then combined with the leaf samples measured in Elsherif, et al. [38], and a third pooled NDI–EWT model was fitted in an attempt to develop a species-independent EWT estimation model for leaves from park environments, collected from different sites. The additional leaf samples included 18 *Acer davidii* (snake-bark maple) leaves, three *Alnus incana* (grey alder) leaves, two lime leaves, one *Alnus glutinosa* (common alder) leaf, one *Populus sp.* (poplar) leaf, and one *Prunus avium* (cherry) leaf. The snake-bark maple leaves were from two nursery trees, while the remaining leaves were from Peel Park, Salford, Manchester, UK. For the October dataset, a pooled NDI–EWT model was fitted to leaf samples from all combined species. In addition, a species-specific model was fitted to holly leaf samples, and a second pooled EWT model was fitted to the remaining species.

2.5. TLS Point-Cloud Processing

The point-cloud processing followed the methodology described in detail by Elsherif, et al. [46]. The registration targets were used to align the P20 and P50 point-clouds of the tree plot on each date using Leica Cyclone version 9.1 (Leica Geosystems HDS). The difference in laser beam footprint and beam divergence between the two instruments resulted in the P20 point-cloud having more points than the corresponding P50 point-cloud. To account for this, a 3D nearest neighbor function was applied in Matlab, which paired each point in the P50 point-cloud with its nearest neighbor in the corresponding P20 point-cloud and then disregarded the remaining points. The intensity was calibrated to reflectance, and then the NDI was calculated on a point-by-point basis, generating an NDI point-cloud of the plot on each date. Individual trees were then manually extracted, and different NDI–EWT models (Section 3.1) were used to generate the EWT point-clouds. The wood components were then manually removed from each tree point-cloud. To validate the EWT estimates, the sections from which leaf samples for validation were collected (0.5 × 0.5 × 0.5 m volume, Section 2.3) were extracted from the corresponding trees in the EWT point-clouds, and the estimated EWT was compared to the actual EWT measured from destructive leaf sampling. Relative errors (E%) were calculated following Equation (3).

$$\text{E\%} = ((\text{estimated EWT} - \text{actual EWT})/\text{actual EWT}) \times 100, \tag{3}$$

The temporal change in EWT (increase/decrease) between August and October was measured for each tree from the TLS estimated EWT, as well as from the destructive sampling EWT, to investigate the accuracy of TLS in detecting such changes. Afterwards, the EWT point-cloud of each tree was split into multiple horizontal layers, 1 m each. The average EWT of each layer was calculated and plotted against height at the center of the layer to produce a vertical profile of the EWT distribution in the canopy. The EWT vertical profiles produced for each tree in the August and October datasets were compared to study how the vertical distribution of EWT temporally varied.

3. Results

3.1. *Leaf Level*

For the August dataset, a high correlation was observed between the NDI and EWT when all leaf samples were combined ($R^2 = 0.7$, $p < 0.05$) (Figure 2). However, the slope and intercept of the NDI–EWT relationship appeared to be affected by the low NDI value (0.08) of one sycamore leaf. Another sycamore leaf also had a lower NDI value than leaves from other species with similar EWT. The two leaves had lower NIR reflectance, 0.31 and 0.36, respectively, than all the other leaf samples, which had NIR reflectance between 0.43 and 0.56. On the other hand, the SWIR reflectance of the two leaves, 0.26 and 0.24, respectively, was within the minimum and maximum values observed in the leaf sampling, 0.19 and 0.35, respectively. The low NDI values were therefore a result of the low NIR reflectance, which could have been caused by the powdery mildew that covered the leaves' surface.

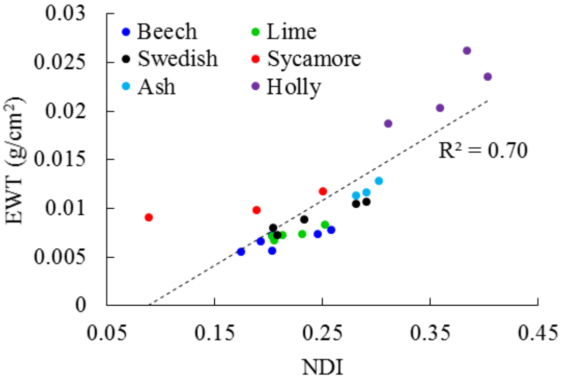

Figure 2. The normalized difference index–equivalent water thickness (NDI–EWT) pooled model in the August dataset. The model was affected by the low NDI value sycamore leaves.

Excluding the sycamore leaves and fitting a second pooled EWT model improved the correlation ($R^2 = 0.88$, $p < 0.05$) (Figure 3, Equation (4)). Similarly, a linear model was fitted to all leaf samples combined in the October dataset ($R^2 = 0.93$, $p < 0.05$) (Figure 3, Equation (5)). Comparing the pooled EWT models on the two different dates showed a similarity in the slopes but a difference in the intercept, with the trendline of the October model being shifted up in comparison to the trendline of the August model. This was likely to be a result of the difference in leaf internal structure between the green leaves (August) and the senescent leaves (October), as senescence can change leaf cell structure [41].

Pooled NDI–EWT models that included holly leaf samples are described as follows:

$$\text{EWT (g cm}^{-2}\text{)} = 0.0925 \times \text{NDI} - 0.0131, \text{ for the August dataset} \tag{4}$$

$$\text{EWT (g cm}^{-2}\text{)} = 0.0852 \times \text{NDI} - 0.0076, \text{ for the October dataset} \tag{5}$$

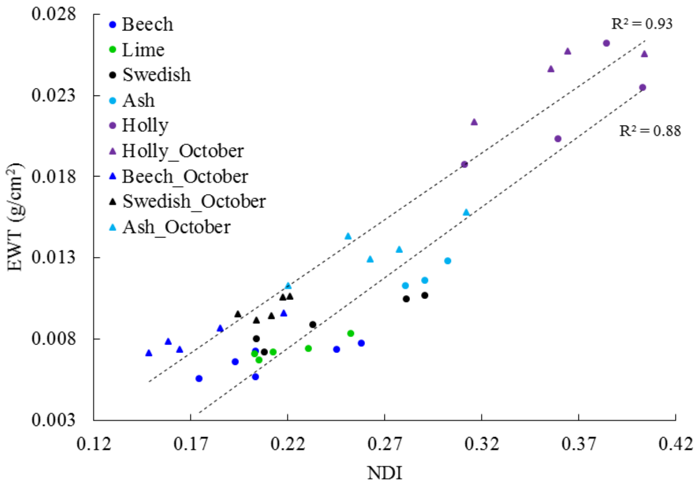

Figure 3. The NDI–EWT pooled model in the August dataset, after excluding the sycamore leaves (bottom), and the NDI–EWT pooled model in the October dataset (top). A shift can be seen between the two trendlines, most likely caused by leaf senescence.

Excluding holly leaf samples from the pooled NDI–EWT model in August and adding the Peel Park leaf samples to the model changed the slope and intercept of the model and improved the correlation (R^2 = 0.92, $p < 0.05$) (Figure 4, Equation (6)). On the other hand, excluding holly leaf samples from the pooled EWT model in the October dataset did not improve the correlation, but it did change the slope and intercept of the model (Figure 4, Equation (7)). The shift in the trendline of the NDI–EWT relationships between August and October remained clear.

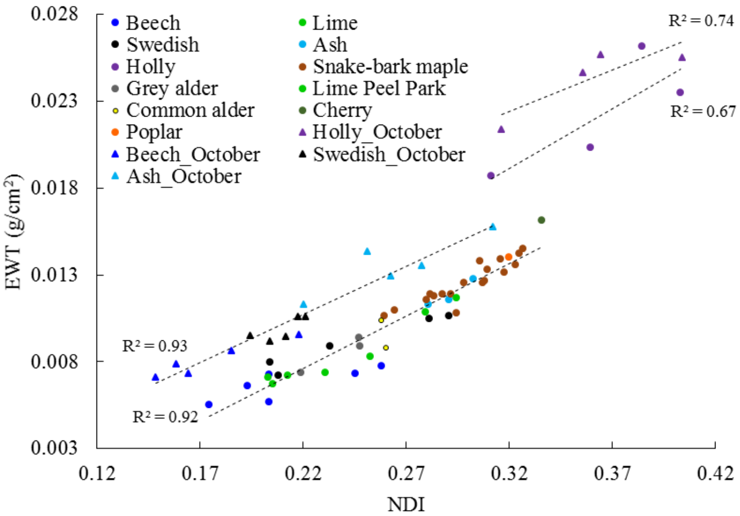

Figure 4. The NDI–EWT pooled model for the August dataset (bottom), after excluding holly leaf samples and adding leaf samples measured by Elsherif, et al. [38], and the NDI–EWT pooled model for the October dataset (top), after excluding holly leaf samples. Holly species-specific NDI–EWT models for August (bottom) and October (top).

Pooled NDI–EWT models that excluded holly leaf samples are described as follows:

$$\text{EWT (g cm}^{-2}\text{)} = 0.0631 \times \text{NDI} - 0.0064, \text{ for the August dataset} \quad (6)$$

$$\text{EWT (g cm}^{-2}\text{)} = 0.0576 \times \text{NDI} - 0.0019, \text{ for the October dataset} \quad (7)$$

Species-specific NDI–EWT models for holly are described as follows:

$$\text{EWT (g cm}^{-2}) = 0.0836 \times \text{NDI} - 0.0083\text{, for the August dataset} \quad (8)$$

$$\text{EWT (g cm}^{-2}) = 0.0558 \times \text{NDI} + 0.0042\text{, for the October dataset} \quad (9)$$

3.2. Canopy Level

Applying the pooled EWT models that included holly leaf samples—Equations (4) and (5) for the August and October datasets, respectively—at the canopy level resulted in low errors in the EWT estimation for holly species but severe errors in the other species except for ash in the October dataset (Table 4). This revealed that although the models had high fitting accuracy ($R^2 = 0.88$ and 0.93 for the August and October datasets, respectively), they did not represent the NDI–EWT relationship at the canopy level for Swedish whitebeam, ash and beech. When the pooled EWT models that excluded holly were used—Equations (6) and (7) for the August and October datasets, respectively—the errors dropped significantly, as shown in Table 4. Thus, care must be taken while fitting a pooled EWT estimation model that is to be applied at the canopy level in a mixed-species plot, and species that have thicker leaves or different surface characteristics than the remaining species may need to be excluded from the model.

Table 4. Errors in EWT estimations for the August and October datasets. Pooled EWT Model 1 refers to the model including holly, while pooled EWT Model 2 is the model excluding holly.

	August		**October**	
	Pooled EWT Model 1	Pooled EWT Model 2	Pooled EWT Model 1	Pooled EWT Model 2
Swedish whitebeam	23.4%	–2.2%	17.8%	6.3%
Ash	25.5%	–4%	–4.2%	–5.6%
Beech	56.2%	12%	–17.6%	7.3%
Holly	1%	4.4% (1)	2.4%	5.8% (1)
Sycamore	–46.7%	—	—	—

(1) EWT was estimated using a species-specific model for holly leaf samples.

In case of the diseased sycamore tree, both pooled EWT models failed to correctly estimate EWT at the canopy level, with the first model producing a severe error in the EWT estimation (–46.7%) and the second model producing a below zero EWT value. Another attempt was made to estimate EWT of the sycamore tree by applying a species-specific sycamore model. However, this also produced severe error in the EWT estimation (–31%). This suggested that this EWT estimation approach can be inapplicable if leaves are covered with a material that does not affect the two wavelengths included in the NDI in a similar manner. Following the unsuccessful attempts to estimate EWT of the sycamore tree, the tree was not included in the October dataset.

Apart from the sycamore tree, high correlation was observed between the estimated EWT and the actual EWT at the canopy level for the combined August and October datasets ($R^2 = 0.98$, $p < 0.05$). A factor contributing to the high correlation was the holly tree having higher EWT than the remaining species in both dates. However, the correlation between the estimated and actual EWT remained high even after excluding holly tree results ($R^2 = 0.94$, $p < 0.05$).

3.3. Temporal Change in EWT

Table 5 shows the change in EWT between August and October for the four trees used in validating the EWT estimates. The destructive sampling results showed an increase in EWT for the Swedish whitebeam, ash and beech trees. The highest increase in EWT was observed in the beech tree, whilst the ash tree showed the least change in EWT between the two dates. On the other hand, some decrease in EWT was observed in the holly tree. However, the change in EWT was measured only for the sections of the trees from which leaf samples for validation were collected and did not necessarily represent the change in EWT for the whole canopy, which would require collecting leaf samples from all canopy layers (see Section 3.4 for EWT vertical profiles). Using TLS to detect the change in EWT resulted in an overestimation of the increase in EWT for the Swedish whitebeam, indicating that EWT increased by 26.7% in this section of the tree, while leaf sampling showed that it only increased by 17.4%, a with 9.3% difference between them. On the other hand, TLS underestimated the increase in EWT for the beech tree, which had an increase in EWT of 20.6% according to leaf sampling and of 15.8% according to TLS (4.8% difference). The change in EWT was detected more accurately for the ash and holly trees, as shown in Table 5, with the difference between actual and estimated EWT change (%) being 1.2% and 1.6%, respectively.

Table 5. Detecting temporal change in EWT between August and October for the four trees used in the EWT estimation validation. A positive sign indicates an increase in EWT, while a negative sign indicates a decrease.

		Swedish Whitebeam	**Ash**	**Beech**	**Holly**
Actual EWT (g cm^{-2}) from leaf sampling	August	0.0092	0.0127	0.0068	0.0266
	October	0.0108	0.0139	0.0082	0.0239
	EWT change	0.0016	0.0012	0.0014	–0.0027
	EWT change (%)	17.4%	9.5%	20.6%	–10.2%
Estimated EWT (g cm^{-2}) from TLS	August	0.0090	0.0121	0.0076	0.0268
	October	0.0114	0.0131	0.0088	0.0245
	EWT change	0.0024	0.0010	0.0012	–0.0023
	EWT change (%)	26.7%	8.3%	15.8%	–8.6%

The change in EWT was also observed in the visual inspection of the point-clouds of the trees on both dates, as shown in Figure 5 for the Swedish whitebeam tree as an example.

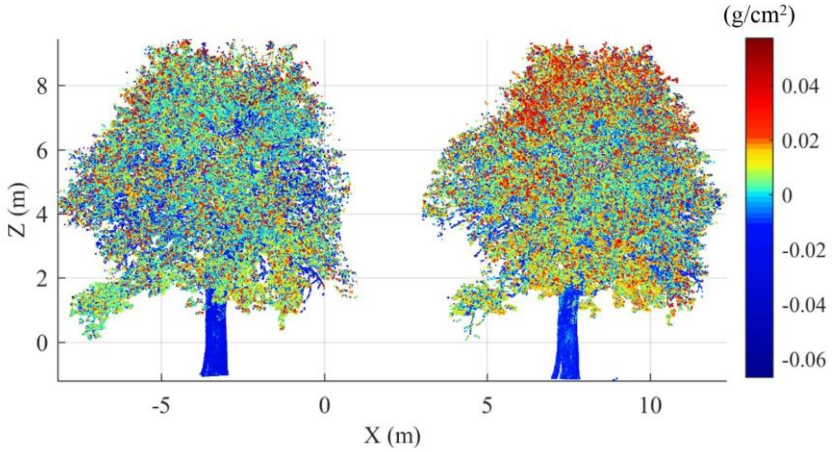

Figure 5. EWT point-clouds of the Swedish whitebeam tree in August (left) and in October (right).

3.4. EWT Vertical Profiles

Figure 6 shows the vertical profiles of EWT for six trees in the plot: Two ash trees, two Swedish whitebeam trees, and two holly trees. The Sycamore tree was excluded following the severe errors in EWT estimation, as discussed in Section 3.2. The beech tree was partially occluded by an ash tree and a holly tree, resulting in few laser beam returns from middle and upper canopy; thus, it was not possible to generate a vertical profile of EWT.

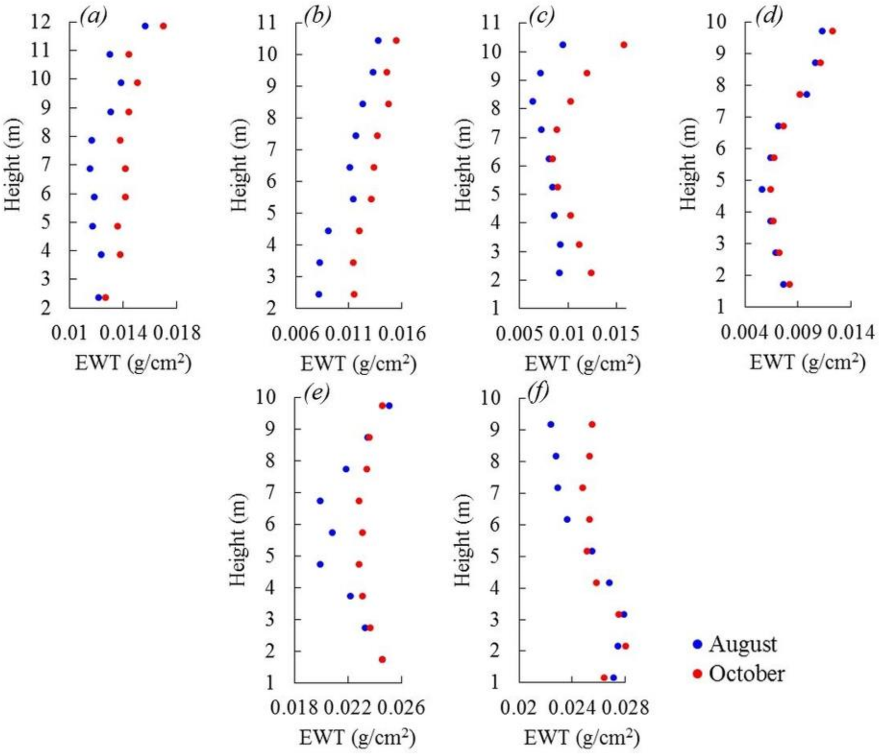

Figure 6. EWT vertical profiles in August (blue) and October (red): (**a**) Ash tree 1; (**b**) Ash tree 2; (**c**) Swedish whitebeam tree 1; (**d**) Swedish Whitebeam tree 2; (**e**) Holly tree 1; and (**f**) Holly tree 2.

Both ash trees had higher EWT in canopy top than in the canopy bottom in August and October. This agreed with the findings reported by Elsherif, et al. [38], Gara, et al. [50] and Zhu, et al. [39] for small, individual trees, and by Chavana-Bryant, et al. [51], Arellano, et al. [52] and Elsherif, et al. [46] for forest canopies, all showing that trees had higher EWT in the canopy top than in the canopy bottom. For ash tree 1, EWT was 29% higher in the canopy top than in the canopy bottom in August, and it was 34% higher in the canopy top than in the canopy bottom in October. For the ash tree 2, EWT was 67% higher in the canopy top in August and 34% higher in the canopy top in October. Both trees had higher EWT in October than in August in all layers, suggesting that when the trees were stressed in August, they lost moisture from all canopy layers. This agreed with the findings reported by Elsherif, et al. [38], where a dry-down experiment was conducted using a snake-bark maple and the change in EWT was monitored using TLS, which showed that the tree lost moisture from all canopy layers.

The Swedish whitebeam trees showed a different behavior to the ash trees. Both trees had higher EWT in the canopy top than in the canopy bottom in both dates, except for tree 1 in August, in which canopy layers between 7 and 10 m had the lowest EWT. However, the vertical profiles of EWT were hourglass shaped, with the lowest EWT being in the middle canopy layers. For tree 1, EWT was higher in October than in August, and comparing the EWT vertical profiles in both dates revealed that there was almost no change in EWT in the middle canopy layers, while EWT increased in the top and bottom layers in October. In August, EWT was higher in the canopy top than in the canopy bottom by only 4%, while it was higher by 27% in October. For tree 2, a slight change in EWT was detected between August and October, with EWT in October being slightly higher. EWT was higher in the canopy top than in the canopy bottom by 48% and 49% in August and October, respectively. The tree was either not affected by the heatwave or had not yet recovered from the stress caused by the drought, considering that, overall, it had lower EWT in October than tree 1.

Similar to the Swedish whitebeam trees, holly tree 1 had hourglass EWT vertical profiles in August and October, with EWT in the middle layers being less than that in the top and bottom of canopy. However, contrary to the behavior observed in Swedish whitebeam tree 1, holly tree 1 maintained the same EWT in the canopy top and canopy bottom during and after the heatwave, while the middle canopy layers showed an increase in EWT in October. On the other hand, holly tree 2 had different EWT vertical profiles than holly tree 1 and also than all the other species. EWT was lower in the canopy top than in the canopy bottom in both August and October. Additionally, there was a slight change in EWT between the two dates in the canopy bottom, while EWT increased in the canopy top in October.

4. Discussion

4.1. Leaf Level

The results obtained at the leaf level highlighted the effect leaf senescence has on the NDI–EWT relationship, which had not previously been investigated in studies that used TLS to estimate EWT, which have only dealt with non-senescent leaves. Senescence changes leaf cell structure [53], and although measuring such changes is a complicated process, PROSPECT simulations can be used to study how these changes affect the NDI–EWT relationship. PROSPECT is a leaf level radiative transfer model that uses the leaf internal structure coefficient (N) to model the cell arrangements in leaf as a number of layers [41]. N typically has a value between 1.5 and 2.5 for non-senescent leaves and >2.5 when leaves are senescent to account for the change in their cellular structure [41]. PROSPECT simulations conducted in Elsherif, et al. [46] showed that an increase in N, while EWT remained constant, could shift the NDI–EWT relationship upward, with the shift becoming more obvious the closer the N value was to 2.5. This can explain the shift in trendlines of the NDI–EWT relationships observed between August and October. Thus, an EWT estimation model developed using non-senescent leaves could not be applied at the canopy level when leaves were senescent, and developing another EWT estimation model using senescent leaves was essential.

A similar concept can be used to explain why holly leaf samples on both dates did not follow the NDI–EWT relationship of the remaining species, and their species-specific NDI–EWT models were also shifted up in comparison to the pooled NDI–EWT model of the remaining species. Holly leaves were clearly thicker than the leaves of the other species, and although their leaf thickness was not measured, their average LMA (0.0164 g cm^{-2}) was 129% higher than the average LMA of ash leaf samples (0.0071 g cm^{-2}), 117% higher than the average LMA of Swedish whitebeam leaf samples (0.0075 g cm^{-2}), and 192% higher than the average LMA of beech leaf samples (0.0056 g cm^{-2}). Gaulton, et al. [43] reported a similar observation when two *Fallopia japonica* (Japanese knotweed) leaf samples were attached together to form a sample with double thickness and were found to deviate from the NDI–EWT relationship of the remaining species. It is worth mentioning that the shiny surface of holly leaf samples could also have been a factor that contributed to the deviation of the NDI–EWT relationship of this species. Zhu, et al. [39] showed that at a 1550 nm wavelength, shiny leaves had stronger specular reflection than matt leaves at a zero incidence angle. A higher reflectance at the 1550 nm wavelength would reduce the NDI value, causing the upward shift of the trendline of the NDI–EWT relationship of holly in comparison to the other matt leaves.

Leaf surface characteristics were also the most likely reason why diseased sycamore leaf samples did not follow the NDI–EWT relationship of the remaining species. The powdery mildew that covered the sycamore leaf samples decreased the NIR reflectance but seemed to have a minimum effect on the SWIR reflectance, as discussed in Section 3.1. Yuan, et al. [54] reported a similar observation in winter wheat, showing a decrease in NIR reflectance and a slight increase in SWIR reflectance in leaves infected with powdery mildew in comparison to healthy leaves. However, powdery mildew in wheat is caused by a different fungus than in sycamore, and further investigation is still needed by scanning healthy and diseased sycamore leaves. As the diseased sycamore leaves appeared to be outliers in the pooled NDI–EWT model, this approach may help in detecting diseased trees in a tree plot, as these trees would appear as outliers in comparison to healthy trees. The results obtained in this study therefore concurred with those previously reported in the literature regarding the NDI–EWT relationship being species-independent to an extent [38,43,46], but highlighted that leaf surface characteristics, leaf senescence, and leaf thickness must be taken in consideration while deriving a pooled, multi-species NDI–EWT model.

4.2. Canopy Level

EWT was successfully estimated across the four different species used in validation on both dates, but this was mainly a factor of applying the correct NDI–EWT estimation model. The errors observed in the EWT estimates were within the range of error expected for this EWT estimation approach, which has been reported in previous studies that used TLS to estimate EWT at the canopy level to be between 1% and 14%, depending on how accurately the NDI–EWT model at the leaf level represented the relationship at the canopy level [38,39,46]. Furthermore, the accuracy of the EWT estimation at the canopy level for the combined August and October datasets (the correlation between estimated and actual EWT, $R^2 = 0.94$) was considered high in comparison to the accuracy reported using optical RS sensors (R^2 ranging between 0.7 and 0.92) [17,55–57]. This can be related to the TLS estimation of EWT being uninfluenced by background soil, understory, and woody materials reflectance. Though the small size of the dataset involved in this study could have also contributed to the high accuracy achieved, the site was heterogeneous and was scanned twice, one of which was during leaf senescence. Such heterogeneous sites are more challenging when it comes to estimating EWT, especially using vegetation indices, because of the variation of canopy LAI (Leaf Area Index) and leaf internal structure between species [17]. Leaf senescence further changes leaf internal structure [41], which can further complicate EWT estimation. However, the accuracy of this EWT estimation approach still needs to be investigated at the plot level for a more representative comparison to the accuracy of the spaceborne and airborne optical RS estimation of EWT. For this method to be applied at the plot level and larger scales, leaf–wood separation algorithms must be used, as manually removing the woody materials is not feasible. The accuracy of estimating canopy EWT at the plot level then depends on how accurately such algorithms can remove the woody materials.

The direction and magnitude of the change in EWT was successfully characterized using TLS in the four sampled trees, showing the potential of this method to be used in detecting the impact of drought on vegetation. With the very high temporal resolution of TLS, which is independent of solar illumination or limited by cloud coverage, it can be used to fill the gaps in time series produced using optical RS spaceborne sensors. The accuracy of detecting the change in EWT appeared to be mainly a function of the EWT estimation errors on both dates. An overestimation or underestimation of EWT in both dates with similar magnitude of errors produced the most accurate estimation of the change in EWT. A higher magnitude of error in one dataset than in the other produced less accurate estimates of the change in EWT, while overestimating EWT in one dataset and underestimating it in the other produced the least accuracy, as observed in the Swedish whitebeam tree. Overall, the errors in August were less than the errors in October, except for the beech tree, which may have been a result of leaf senescence. The senescence effect on leaf internal structure is known to vary between species, and it can also vary between leaves from the same species if they are at different levels of senescence [53]. Thus, it can be more challenging to build an NDI–EWT model that can accurately represent all levels of senescence in a plot. Another source of errors was the wind effect. Though the plot was scanned in non-windy conditions on both dates, there was a gentle breeze in October during the scan. This may have reduced the accuracy of aligning the point-clouds from the two instruments in the October dataset, leading to higher errors in estimating EWT on a point-by-point basis. However, this was not obvious in the RMSE (Root Mean Squared Error) of the point-clouds alignment, which was 3 mm in both datasets.

4.3. EWT Vertical Profiles

Vertical heterogeneity in EWT within the canopy was observed in all six trees examined. This concurred with the findings reported in the few studies found in the literature that have investigated the vertical distribution of EWT at the canopy level [38,39,46,50,52,58,59]. The EWT vertical profiles and their temporal changes varied within and between species, and such measurements could not be obtained using optical RS spaceborne and airborne sensors. The results showed that the presented method can help improve understanding of 3D biochemistry and resource allocation in trees, and it could provide new insights into how trees react to heatwaves and droughts.

One reason for the observed EWT heterogeneity is that leaves at different heights within the canopy contribute differently to the total canopy photosynthesis and carbon storage [60,61], and trees tend to dedicate more nutrients and water to the well-illuminated leaves in the canopy top (known as sun leaves) than to the shaded leaves in the canopy bottom to optimize photosynthesis [62,63]. This can explain the behavior observed in the two ash trees involved in this study, in which EWT was higher in the canopy top, gradually getting lower towards the canopy bottom. However, this was not the case for the Swedish whitebeam and holly trees, which had different EWT vertical profiles in which EWT was not always the highest in the canopy top and the lowest in the canopy bottom. Typically, sun leaves grow in the canopy top because the top layers of the canopy receive the majority of irradiance [64]. However, in the plot scanned in this study, there was a wide gap in the canopy in the middle of the plot; thus, sun leaves were not necessarily only in the canopy top, depending on how the trees were illuminated. Holly leaf samples further confirmed this, as holly is known to be able to grow different types of leaves depending on the position of leaves in the canopy, with shaded, canopy bottom leaves having sharp prickles to protect them from animals and insects and sun leaves being smaller and smoother [65]. However, despite all leaf samples being collected from the canopy bottom in both dates, among the eighteen leaf samples collected, only four were prickly and fourteen were smooth, suggesting that the canopy bottom layers were sun leaves. This can explain why the two holy trees in the plot had high EWT in the canopy bottom layers and also attempted to maintain unchanged EWT in these layers when the trees were stressed, all while losing moisture from the middle canopy layers in holly tree 1 and from the canopy top in holly tree 2.

The EWT vertical profiles could also be a result of the LMA distribution within the canopy, as EWT and the LMA were reported to be highly correlated, suggesting that a leaf with a higher LMA, typically thicker, is able to hold more moisture than a thinner leaf of the same species [45,46]. Arellano, et al. [52] and Gara, et al. [50] also reported that the EWT and LMA vertical profiles showed similarities, with canopy layers with a higher LMA having higher EWT. This can again be related to the illumination conditions and the distribution of sun/shade leaves within canopy, as sun leaves are typically thicker and have a higher LMA than shade leaves [66].

5. Conclusions

This study investigated the potential of using dual-wavelength TLS to monitor the change in EWT at the canopy level in 3D, during and after a heatwave, in a mixed-species tree plot. An NDI of 808 and 1550 nm wavelengths with the Leica P20 and Leica P50 TLS instruments was found to be highly correlated to EWT at the leaf level, but senescent and green leaves, even from the same species, could not be combined in a pooled NDI–EWT model, most likely because of the change in leaf internal structure caused by senescence. Furthermore, diseased sycamore leaves, covered with powdery mildew, and holly leaves, with waxy, glossy surface, did not follow the NDI–EWT relationship of the remaining species, which could have been a result of the different surface characteristics or spectral properties of their leaves. At the canopy level, EWT was estimated with 6% relative error, and the change in EWT (%) was estimated using destructive leaf sampling and TLS. The accuracy of detecting the change in EWT using TLS varied depending on the errors in the EWT estimates on both dates.

EWT vertical profiles showed heterogeneity in all trees, but EWT was not always higher in the canopy top than in canopy bottom as reported in previous studies in the literature. The vertical profiles varied between species and also between individual trees from the same species, and the illumination conditions, caused by the wide canopy gap in the middle of the plot, may have caused this variation. Illumination conditions are a factor that contribute to the locations of sun and shade leaves in a canopy, and this factor affects the distribution of the LMA within canopy, as well as the distribution of EWT as a result. The change in EWT vertical profiles between and after the heatwave also varied, not only between species but also between individual trees. This showed that trees reacted differently to the drought condition, maintaining constant EWT in specific canopy layers, most likely because these layers contributed the most to photosynthesis.

This study showed the potential of using dual-wavelength TLS to detect temporal changes in EWT, and it also revealed the new insights TLS can provide about moisture content distribution within the canopy, as well as how different species and different trees change the distribution of EWT during drought conditions to optimize photosynthesis and ensure the survival of the plant. TLS can provide more information about canopy structure and biochemistry than multispectral and hyperspectral cameras that suffer from occlusion in dense vegetation canopies. However, the applicability of this method in a real forest environment still needs to be investigated, as the errors in EWT estimates in such environments were reported to vary between species and between individual trees, which can reduce the accuracy of detecting the change in EWT between two different datasets. The method also needs to be tested on a larger scale, at the plot level, in order to be compared to time series produced using spaceborne and airborne optical RS sensors.

Author Contributions: Conceptualization, A.E., R.G. and J.M.; methodology, A.E., R.G. and J.M.; software, A.E.; validation, A.E., R.G. and J.M.; writing—original draft preparation, A.E.; writing—review and editing, A.E., R.G. and J.M.; and supervision, R.G. and J.M.

Funding: This research was funded by the Ministry of Higher Education, Egypt, represented by the Egyptian Cultural and Educational Bureau in London, UK, as part of A.E. PhD scholarship. The research also made use of equipment funded by UKCRIC—UK Collaboratorium for Research in Infrastructure & Cities: Newcastle Laboratories (EPSRC award EP/R010102/1).

Acknowledgments: The authors would like to thank Hexagon Geosystems for loan of the Leica P50 scanner used in the experiments.

Conflicts of Interest: The authors declare no conflict of interest. The funders had no role in the design of the study; in the collection, analyses, or interpretation of data; in the writing of the manuscript, or in the decision to publish the results.

References

1. Schär, C.; Vidale, P.L.; Lüthi, D.; Frei, C.; Häberli, C.; Liniger, M.A.; Appenzeller, C. The role of increasing temperature variability in European summer heatwaves. *Nature* **2004**, *427*, 332. [CrossRef] [PubMed]
2. Allen, C.D.; Breshears, D.D.; McDowell, N.G. On underestimation of global vulnerability to tree mortality and forest die-off from hotter drought in the anthropocene. *Ecosphere* **2015**, *6*, 1–55. [CrossRef]
3. García-Herrera, R.; Díaz, J.; Trigo, R.M.; Luterbacher, J.; Fischer, E.M. A review of the european summer heat wave of 2003. *Crit. Rev. Environ. Sci. Technol.* **2010**, *40*, 267–306. [CrossRef]
4. Stott, P.A.; Stone, D.A.; Allen, M.R. Human contribution to the European heatwave of 2003. *Nature* **2004**, *432*, 610. [CrossRef] [PubMed]
5. Vogel, M.M.; Zscheischler, J.; Wartenburger, R.; Dee, D.; Seneviratne, S.I. Concurrent 2018 hot extremes across northern hemisphere due to human-induced climate change. *Earth's Future* **2019**, *7*, 692–703. [CrossRef]
6. Mitchell, D.; Kornhuber, K.; Huntingford, C.; Uhe, P. The day the 2003 European heatwave record was broken. *Lancet Planet. Health* **2019**, *3*, e290–e292. [CrossRef]
7. Ceccato, P.; Flasse, S.; Tarantola, S.; Jacquemoud, S.; Grégoire, J.-M. Detecting vegetation leaf water content using reflectance in the optical domain. *Remote Sens. Environ.* **2001**, *77*, 22–33. [CrossRef]
8. Jarvis, P.G.; McNaughton, K. Stomatal control of transpiration: Scaling up from leaf to region. In *Advances in Ecological Research*; Elsevier: London, UK, 1986; Volume 15, pp. 1–49.
9. Farquhar, G.D.; Sharkey, T.D. Stomatal conductance and photosynthesis. *Annu. Rev. Plant Physiol.* **1982**, *33*, 317–345. [CrossRef]
10. Bartlett, M.K.; Klein, T.; Jansen, S.; Choat, B.; Sack, L. The correlations and sequence of plant stomatal, hydraulic, and wilting responses to drought. *Proc. Natl. Acad. Sci. USA* **2016**, *113*, 13098–13103. [CrossRef] [PubMed]
11. McDowell, N.G.; Fisher, R.A.; Xu, C.; Domec, J.; Hölttä, T.; Mackay, D.S.; Sperry, J.S.; Boutz, A.; Dickman, L.; Gehres, N. Evaluating theories of drought-induced vegetation mortality using a multimodel–experiment framework. *New Phytol.* **2013**, *200*, 304–321. [CrossRef] [PubMed]

12. Sepulcre-Cantó, G.; Zarco-Tejada, P.J.; Jiménez-Muñoz, J.; Sobrino, J.; De Miguel, E.; Villalobos, F.J. Detection of water stress in an olive orchard with thermal remote sensing imagery. *Agric. For. Meteorol.* **2006**, *136*, 31–44. [CrossRef]
13. Yebra, M.; Chuvieco, E.; Riaño, D. Estimation of live fuel moisture content from modis images for fire risk assessment. *Agric. For. Meteorol.* **2008**, *148*, 523–536. [CrossRef]
14. Clevers, J.G.P.W.; Kooistra, L.; Schaepman, M.E. Estimating canopy water content using hyperspectral remote sensing data. *Int. J. Appl. Earth Obs. Geoinf.* **2010**, *12*, 119–125. [CrossRef]
15. Ceccato, P.; Gobron, N.; Flasse, S.; Pinty, B.; Tarantola, S. Designing a spectral index to estimate vegetation water content from remote sensing data: Part 1—Theoretical approach. *Remote Sens. Environ.* **2002**, *82*, 188–197. [CrossRef]
16. Tucker, C.J. Remote sensing of leaf water content in the near infrared. *Remote Sens. Environ.* **1980**, *10*, 23–32. [CrossRef]
17. Zarco-Tejada, P.J.; Rueda, C.A.; Ustin, S.L. Water content estimation in vegetation with modis reflectance data and model inversion methods. *Remote Sens. Environ.* **2003**, *85*, 109–124. [CrossRef]
18. Hunt, J.E.; Rock, B. Detection of changes in leaf water content using near- and middle-infrared reflectance. *Remote Sens. Environ.* **1989**, *30*, 43–54.
19. Hardisky, M.; Klemas, V.; Smart, M. The influence of soil salinity, growth form, and leaf moisture on the spectral radiance of. *Spartina Alterniflora* **1983**, *49*, 77–83.
20. Gao, B.C. Ndwi—A normalised difference water index for remote sensing of vegetation liquid water from space. *Remote Sens. Environ.* **1996**, *58*, 257–266. [CrossRef]
21. Peñuelas, J.; Filella, I.; Biel, C.; Serrano, L.; Save, R. The reflectance at the 950–970 nm region as an indicator of plant water status. *Int. J. Remote Sens.* **1993**, *14*, 1887–1905. [CrossRef]
22. Chen, D.; Huang, J.; Jackson, T.J. Vegetation water content estimation for corn and soybeans using spectral indices derived from modis near-and short-wave infrared bands. *Remote Sens. Environ.* **2005**, *98*, 225–236. [CrossRef]
23. Rodríguez-Pérez, J.R.; Riaño, D.; Carlisle, E.; Ustin, S.; Smart, D.R. Evaluation of hyperspectral reflectance indexes to detect grapevine water status in vineyards. *Am. J. Enol. Vitic.* **2007**, *58*, 302–317.
24. Fensholt, R.; Sandholt, I. Derivation of a shortwave infrared water stress index from modis near-and shortwave infrared data in a semiarid environment. *Remote Sens. Environ.* **2003**, *87*, 111–121. [CrossRef]
25. Yebra, M.; Dennison, P.E.; Chuvieco, E.; Riano, D.; Zylstra, P.; Hunt, E.R., Jr.; Danson, F.M.; Qi, Y.; Jurdao, S. A global review of remote sensing of live fuel moisture content for fire danger assessment: Moving towards operational products. *Remote Sens. Environ.* **2013**, *136*, 455–468. [CrossRef]
26. Ali, A.M.; Darvishzadeh, R.; Skidmore, A.K.; Duren, I.V. Effects of canopy structural variables on retrieval of leaf dry matter content and specific leaf area from remotely sensed data. *J. Sel. Top. Appl. Earth Obs. Remote Sens.* **2016**, *9*, 898–909. [CrossRef]
27. Eitel, J.U.H.; Vierling, L.A.; Long, D.S. Simultaneous measurements of plant structure and chlorophyll content in broadleaf saplings with a terrestrial laser scanner. *Remote Sens. Environ.* **2010**, *114*, 2229–2237. [CrossRef]
28. Serrano, L.; Ustin, S.L.; Roberts, D.A.; Gamon, J.A.; Penuelas, J. Deriving water content of chaparral vegetation from aviris data. *Remote Sens. Environ.* **2000**, *74*, 570–581. [CrossRef]
29. Baret, F.; Guyot, G. Potentials and limits of vegetation indices for lai and apar assessment. *Remote Sens. Environ.* **1991**, *35*, 161–173. [CrossRef]
30. Jacquemoud, S.; Baret, F.; Andrieu, B.; Danson, F.; Jaggard, K. Extraction of vegetation biophysical parameters by inversion of the prospect+ sail models on sugar beet canopy reflectance data. Application to tm and aviris sensors. *Remote Sens. Environ.* **1995**, *52*, 163–172. [CrossRef]
31. Kötz, B.; Schaepman, M.; Morsdorf, F.; Bowyer, P.; Itten, K.; Allgöwer, B. Radiative transfer modeling within a heterogeneous canopy for estimation of forest fire fuel properties. *Remote Sens. Environ.* **2004**, *92*, 332–344. [CrossRef]
32. Ustin, S.L.; Roberts, D.A.; Pinzon, J.; Jacquemoud, S.; Gardner, M.; Scheer, G.; Castaneda, C.M.; Palacios-Orueta, A. Estimating canopy water content of chaparral shrubs using optical methods. *Remote Sens. Environ.* **1998**, *65*, 280–291. [CrossRef]
33. White, K.; Pontius, J.; Schaberg, P. Remote sensing of spring phenology in northeastern forests: A comparison of methods, field metrics and sources of uncertainty. *Remote Sens. Environ.* **2014**, *148*, 97–107. [CrossRef]

34. Eastman, J.; Sangermano, F.; Machado, E.; Rogan, J.; Anyamba, A. Global trends in seasonality of normalized difference vegetation index (ndvi), 1982–2011. *Remote Sens.* **2013**, *5*, 4799–4818. [CrossRef]
35. Améglio, T.; Archer, P.; Cohen, M.; Valancogne, C.; Daudet, F.-A.; Dayau, S.; Cruiziat, P. Significance and limits in the use of predawn leaf water potential for tree irrigation. *Plant. Soil* **1999**, *207*, 155–167. [CrossRef]
36. Wang, Q.; Li, P. Canopy vertical heterogeneity plays a critical role in reflectance simulation. *Agric. For. Meteorol.* **2013**, *169*, 111–121. [CrossRef]
37. Kuusk, A. A two-layer canopy reflectance model. *J. Quant. Spectrosc. Radiat. Transf.* **2001**, *71*, 1–9. [CrossRef]
38. Elsherif, A.; Gaulton, R.; Mills, J. Estimation of vegetation water content at leaf and canopy level using dual-wavelength commercial terrestrial laser scanners. *Interface Focus* **2018**, *8*, 59–69. [CrossRef]
39. Zhu, X.; Wang, T.; Skidmore, A.K.; Darvishzadeh, R.; Niemann, K.O.; Liu, J. Canopy leaf water content estimated using terrestrial lidar. *Agric. For. Meteorol.* **2017**, *232*, 152–162. [CrossRef]
40. Hancock, S.; Gaulton, R.; Danson, F.M. Angular reflectance of leaves with a dual-wavelength terrestrial lidar and its implications for leaf-bark separation and leaf moisture estimation. *IEEE Trans. Geosci. Remote Sens.* **2017**, *55*, 3084–3090. [CrossRef]
41. Jacquemoud, S.; Baret, F. Prospect—A model of leaf optical-properties spectra. *Remote Sens. Environ.* **1990**, *34*, 75–91. [CrossRef]
42. Kaasalainen, S.; Åkerblom, M.; Nevalainen, O.; Hakala, T.; Kaasalainen, M. Uncertainty in multispectral lidar signals caused by incidence angle effects. *Interface Focus* **2018**, *8*, 20170033. [CrossRef] [PubMed]
43. Gaulton, R.; Danson, F.M.; Ramirez, F.A.; Gunawan, O. The potential of dual-wavelength laser scanning for estimating vegetation moisture content. *Remote Sens. Environ.* **2013**, *132*, 32–39. [CrossRef]
44. Junttila, S.; Sugano, J.; Vastaranta, M.; Linnakoski, R.; Kaartinen, H.; Kukko, A.; Holopainen, M.; Hyyppä, H.; Hyyppä, J. Can leaf water content be estimated using multispectral terrestrial laser scanning? A case study with norway spruce seedlings. *Front. Plant Sci.* **2018**, *9*, 299. [CrossRef] [PubMed]
45. Junttila, S.; Holopainen, M.; Vastaranta, M.; Lyytikäinen-Saarenmaa, P.; Kaartinen, H.; Hyyppä, J.; Hyyppä, H. The potential of dual-wavelength terrestrial lidar in early detection of ips typographus (L.) infestation–leaf water content as a proxy. *Remote Sens. Environ.* **2019**, *231*, 111264. [CrossRef]
46. Elsherif, A.; Gaulton, R.; Shenkin, A.; Malhi, Y.; Mills, J. Three dimensional mapping of forest canopy equivalent water thickness using dual-wavelength terrestrial laser scanning. *Agric. For. Meteorol.* **2019**, *276*, 107627. [CrossRef]
47. Elsherif, A.; Gaulton, R.; Mills, J. The potential of dual-wavelength terrestrial laser scanning in 3d canopy fuel moisture content mapping. In Proceedings of the ISPRS Geospatial Week 2019, Enschede, The Netherlands, 10–14 June 2019.
48. Schneider, C.A.; Rasband, W.S.; Eliceiri, K.W. Nih image to imagej: 25 Years of image analysis. *Nat. Methods* **2012**, *9*, 671–675. [CrossRef]
49. Danson, F.M.; Steven, M.D.; Malthus, T.J.; Clark, J.A. High-spectral resolution data for determining leaf water content. *Int. J. Remote Sens.* **1992**, *13*, 461–470. [CrossRef]
50. Gara, T.W.; Darvishzadeh, R.; Skidmore, A.K.; Wang, T. Impact of vertical canopy position on leaf spectral properties and traits across multiple species. *Remote Sens.* **2018**, *10*, 346. [CrossRef]
51. Chavana-Bryant, C.; Malhi, Y.; Wu, J.; Asner, G.P.; Anastasiou, A.; Enquist, B.J.; Caravasi, C.; Eric, G.; Doughty, C.E.; Saleska, S.R. Leaf aging of amazonian canopy trees as revealed by spectral and physiochemical measurements. *New Phytol.* **2016**, *214*, 1049–1063. [CrossRef]
52. Arellano, P.; Tansey, K.; Balzter, H.; Boyd, D.S. Field spectroscopy and radiative transfer modelling to assess impacts of petroleum pollution on biophysical and biochemical parameters of the amazon rainforest. *Environ. Earth Sci.* **2017**, *76*, 217. [CrossRef]
53. Buchanan-Wollaston, V. The molecular biology of leaf senescence. *J. Exp. Bot.* **1997**, *48*, 181–199. [CrossRef]
54. Yuan, L.; Huang, Y.; Loraamm, R.W.; Nie, C.; Wang, J.; Zhang, J. Spectral analysis of winter wheat leaves for detection and differentiation of diseases and insects. *Field Crop. Res.* **2014**, *156*, 199–207. [CrossRef]
55. Yilmaz, M.T.; Hunt, E.R., Jr.; Jackson, T.J. Remote sensing of vegetation water content from equivalent water thickness using satellite imagery. *Remote Sens. Environ.* **2008**, *112*, 2514–2522. [CrossRef]
56. Champagne, C.M.; Staenz, K.; Bannari, A.; McNairn, H.; Deguise, J.-C. Validation of a hyperspectral curve-fitting model for the estimation of plant water content of agricultural canopies. *Remote Sens. Environ.* **2003**, *87*, 148–160. [CrossRef]

57. Cheng, Y.-B.; Ustin, S.L.; Riaño, D.; Vanderbilt, V.C. Water content estimation from hyperspectral images and modis indexes in southeastern Arizona. *Remote Sens. Environ.* **2008**, *112*, 363–374. [CrossRef]
58. Zhang, Y.; Zhu, H.; Yan, B.; Ou, Y.; Li, X. Vertical distribution and temporal variation of nitrogen, phosphorus and carbon in ditch sediment of Sanjiang plain northeast china. *Fresenius Environ. Bull.* **2013**, *22*, 2265–2272.
59. Liu, S.; Peng, Y.; Wei, D.; Le, Y.; Li, L. Remote estimation of leaf and canopy water content in winter wheat with different vertical distribution of water-related properties. *Remote Sens.* **2015**, *7*, 4626–4650. [CrossRef]
60. Aber, J.D. Foliage-height profiles and succession in northern hardwood forests. *Ecology* **1979**, *60*, 18–23. [CrossRef]
61. Ellsworth, D.; Reich, P. Canopy structure and vertical patterns of photosynthesis and related leaf traits in a deciduous forest. *Oecologia* **1993**, *96*, 169–178. [CrossRef]
62. Hikosaka, K. Leaf canopy as a dynamic system: Ecophysiology and optimality in leaf turnover. *Ann. Bot.* **2004**, *95*, 521–533. [CrossRef]
63. Hirose, T.; Werger, M. Maximizing daily canopy photosynthesis with respect to the leaf nitrogen allocation pattern in the canopy. *Oecologia* **1987**, *72*, 520–526. [CrossRef] [PubMed]
64. Chazdon, R.L.; Fetcher, N. Photosynthetic light environments in a lowland tropical rain forest in Costa Rica. *J. Ecol.* **1984**, 553–564. [CrossRef]
65. Herrera, C.M.; Bazaga, P. Epigenetic correlates of plant phenotypic plasticity: DNA methylation differs between prickly and nonprickly leaves in heterophyllous ilex aquifolium (aquifoliaceae) trees. *Bot. J. Linn. Soc.* **2013**, *171*, 441–452. [CrossRef]
66. Lichtenthaler, H.K.; Buschmann, C.; Döll, M.; Fietz, H.J.; Bach, T.; Kozel, U.; Meier, D.; Rahmsdorf, U. Photosynthetic activity, chloroplast ultrastructure, and leaf characteristics of high-light and low-light plants and of sun and shade leaves. *Photosynth. Res.* **1981**, *2*, 115–141. [CrossRef] [PubMed]